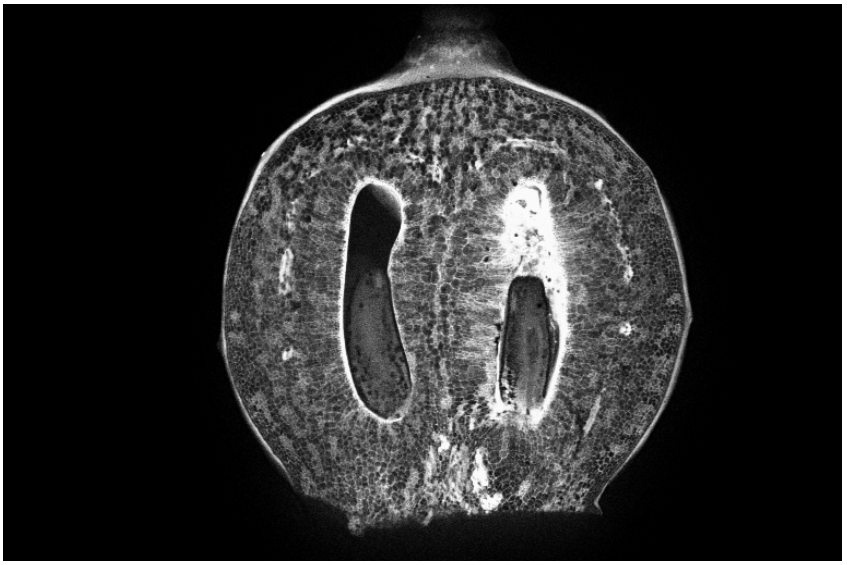
SOUTHCORP WINES

The basis of variation in size and composition of grape berries



FINAL REPORT to

GRAPE AND WINE RESEARCH & DEVELOPMENT CORPORATION

Project Number:

Principal Investigator: **John D.**

Research Organisation: **The University of Adelaide**

Date: **27/7/01**

UA 95/1

SUMMARY

The size and composition of grape berries is determined during the early stages of berry development by factors that govern cell division and cell expansion. Variation in berry size and composition is due to variability in these developmental processes. The aim of this study was to establish a methodology that would allow precise three-dimensional measurements of cell size *in situ.* The method uses confocal laser scanning microscopy and digital image reconstruction to visualise cells in whole mounts of cleared, stained berry tissues. Cells from the inner mesocarp of a single berry exhibited a much wider range of sizes and shapes than had previously been observed.

This report is based on the following publication (reproduced with permission of Blackwell Science):

Gray, J.D., Kolesik, P., Høj, P.B. and Coombe, B.G. (1999). Confocal measurement of the three-dimensional size and shape of plant parenchyma cells in a developing fruit tissue. *The Plant Journal,* **19,** 229-236.

Confocal Measurement of the Three-Dimensional Size and Shape of Plant Parenchyma Cells in a Developing Fruit Tissue

John D. Gray[1,*], Peter Kolesik[1], Peter B. Høj[1,2] and Bryan G. Coombe[1]

[1] Department of Horticulture, Viticulture and Oenology, Waite Campus, The University of Adelaide, Glen Osmond, SA 5064, Australia

[2] Australian Wine Research Institute, Glen Osmond, SA 5064, Australia

[*] For correspondence (CSIRO Plant Industry, Horticulture Unit, Merbein Laboratory, Merbein, VIC 3505, Australia. Fax +61 35051 3111. E-mail john.gray@pi.csiro.au).

SUMMARY

Parenchyma cells from the inner mesocarp of a grape berry (*Vitis vinifera* L. cv. Chardonnay) were visualised in three-dimensions within a whole mount of cleared, stained tissue using confocal laser scanning microscopy and digital image reconstruction. The whole berry was fixed, bisected longitudinally, cleared in methyl salicylate, stained with safranin O and mounted in methyl salicylate. Optical slices were collected at 1.0 µm intervals to a depth of 150 µm. Neighbouring z-series were joined post-collection to double the field of view. Attenuation at depth of the fluorescent signal from cell walls was quantified and corrected. Axial distortion due to refractive index mismatch between the immersion and mounting media was calibrated using yellow-green fluorescent microspheres, and corrected. Transmission electron microscopy was used to correct fluorescent measurements of cell wall thickness. Digital image reconstructions of wall-enclosed spaces enabled cells to be rendered as geometric solids of measurable surface area and volume. Cell volumes within the inner mesocarp tissue of a single grape berry exhibited a fourteen-fold range, with polysigmoidal distribution and groupings around specific size classes. Cell shape was irregular and the planes of contact were rarely flat or simple. Variability in cell shape was indicated by the range in surface area to volume ratios, from 0.080 to 0.198 μm^{-1}. Structural detail at the internal surface of the cell wall was apparent. The technique is applicable to a wide range of morphometric analyses in plant cell biology, particularly developmental studies, and reveals details of cell size and shape that were previously unattainable.

l, wavelength; **3D,** three-dimensional; **CLSM,** confocal laser scanning microscopy; **FPA_{50},** formalin:propionic acid:50% ethanol 1:1:18; **GMA,** glycol methacrylate; **NA,** numerical aperture; **RI,** refractive index; **TEM,** transmission electron microscopy

INTRODUCTION

Elucidation of the relative positioning, shape and size of plant parenchyma cells *in situ* has hitherto been achieved by indirect methods involving microscopic analyses of thin, serial sections followed by stereological analysis (Considine, 1978; 1981; Cruz-Orive, 1997; Møller *et al.*, 1990; Underwood, 1970; Weibel, 1979; 1980) or three-dimensional (3D)

reconstruction of physical slices (Bron *et al.*, 1990; Korn, 1974; Korn and Spalding, 1973; Lewis, 1926; Matzke, 1948; Williams, 1968). While appropriate for tissues composed of isodiametric cells, stereological methods underestimate mean cell sizes (Considine and Knox, 1981) and do not allow accurate determinations of intra-tissue variation (Parsons *et al.*, 1989). Although 3D reconstruction of serial sections has yielded invaluable insights into the organisation of cells in specific tissues (e.g. Williams, 1970), the methodology has limitations due to artefacts introduced during the preparation of tissue slices and the subsequent tedious reconstruction.

It is desirable that methods be adopted for investigating cells within tissues in which physical sectioning is not required. The recent development of confocal laser scanning microscopy (CLSM) allows this possibility. Whole mounts of cleared, stained tissue in combination with optical sectioning by CLSM and digital 3D image reconstruction offers an alternative to conventional techniques.

CLSM combines laser light illumination, fluorescence microscopy and computer imaging. Under ideal circumstances it has sharp depth discrimination and produces horizontal optical slices of tissues in the plane of focus (Pawley, 1995). The resultant images are digitised and stored as a vertical image stack, or z-series. Digital 3D image reconstruction enables the z-series to be visualised as a geometric structure (Carlsson *et al.*, 1985; Yu *et al.*, 1994). Applications of CLSM to the study of plant microstructure include 3D reconstruction of guard cells in *Commelina* leaves (White *et al.*, 1996), the measurement of cell wall thickness in spring barley and maize (Travis *et al.*, 1997), and *in vivo* observation of sieve tubes in fava bean leaves (Knoblauch and van Bel, 1998).

In this study we describe a further development for the detailed study of plant cell morphology and organisation using as object the parenchyma cells of the inner mesocarp of the grape berry. The combination of traditional clearing procedures with confocal microscopy enabled entire parenchyma cells (wall-enclosed spaces) to be visualised and measured *in situ.* The technique was tested on a number of berries of different ages. The images and measurements presented in this paper pertain to a collection of parenchyma cells from a single tissue block within one young grape berry (cv. Chardonnay, 26 days after anthesis, 5 mm diameter).

RESULTS

Staining and Mounting the Tissue Block

Fluorescence, either autofluorescence or stain induced, is a pre-requisite to imaging cell walls under CLSM. Autofluorescence of berry cell walls was heterogeneous therefore staining was needed to induce even fluorescence. Of the 16 stains tested, the majority gave poor or incomplete fluorescence of cell walls. Safranin O was adopted because it exhibited adequate labelling, suitable wavelengths of excitation and emission, and resistance to photobleaching. Methyl salicylate proved the most successful clearing medium: tissue distortion appeared to be minimal and the entire berry half was transparent under bright-field illumination. The adopted mounting procedure is shown in Figure 1.

Visualising Cell Walls

The tissue was imaged to a depth of 150 µm with the CSLM. The 151 optical slices which comprised the confocal z-series indicated the high degree of resolution attainable. Parenchyma cell walls were clearly visible in the consecutive optical slices, 1.0 µm apart, shown in Figure 2. Membranous structures visible within certain cells indicated possible plasmolysis. Despite this, cell walls remained intact and no intercellular spaces were apparent.

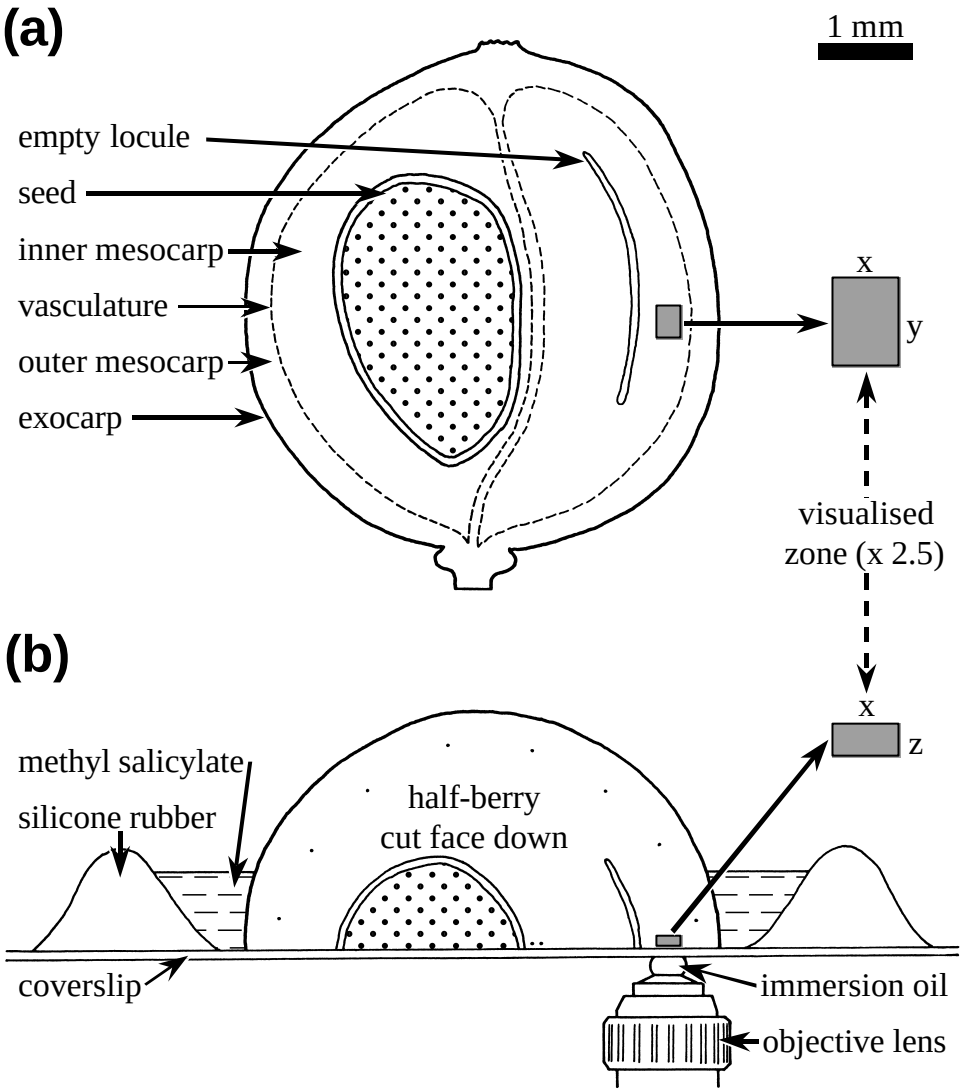


Figure 1. Grape berry tissues. Diagram of young grape berry showing location of tissues and zone viewed by CLSM (berry and zone to scale). (a) Longitudinally cut surface of the berry. (b) Section of stained and cleared half-berry positioned cut face down on coverslip in a well constructed of silicone rubber filled with methyl salicylate. The dimensions of the visualised zone are x = 289 µm, y = 385 µm, z = 150 µm.

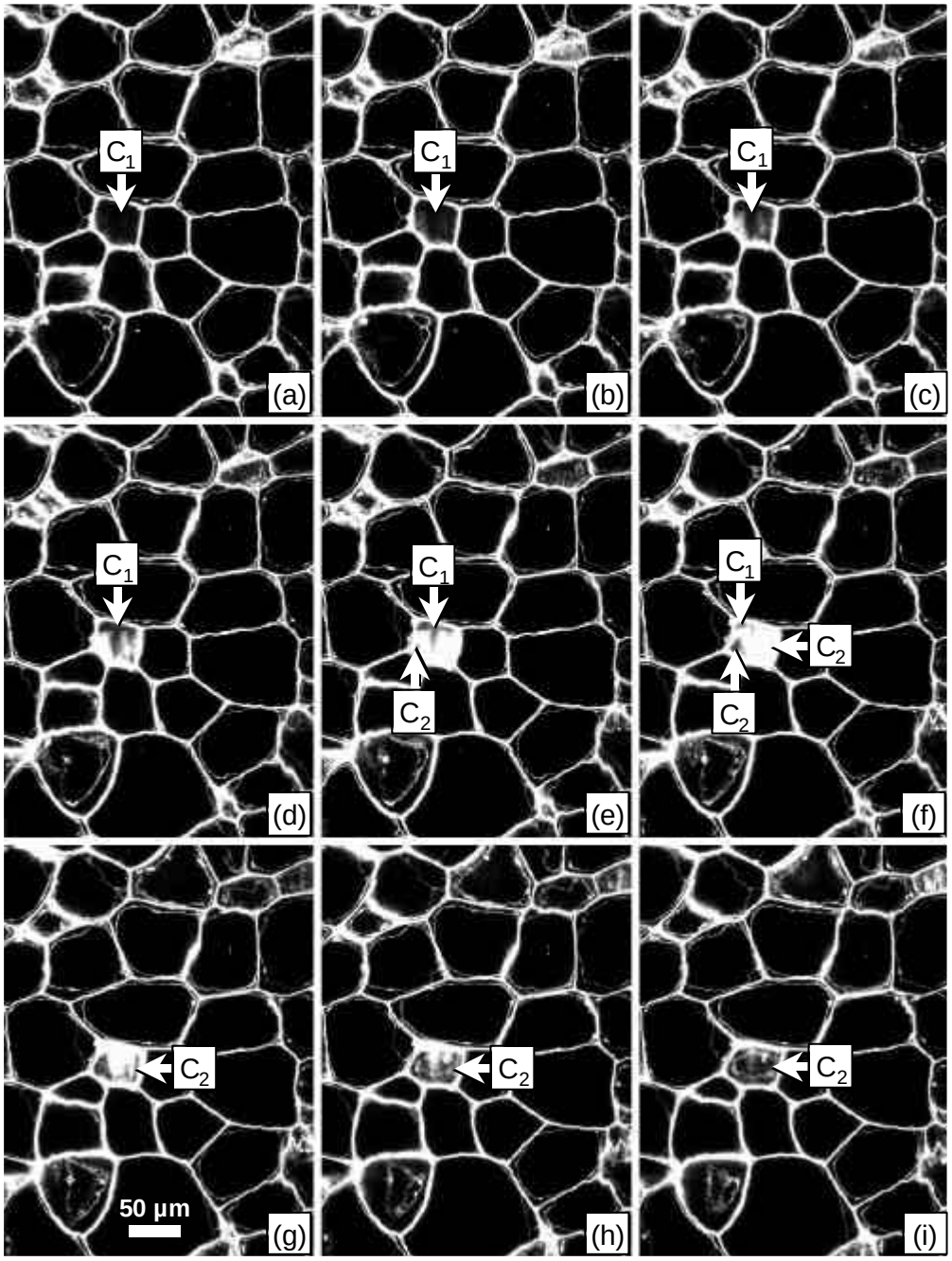


Figure 2. Optical slices of parenchyma cells. (a-i) Consecutive optical slices, 1.0 µm apart, through a block of parenchyma tissue of the inner mesocarp of a Chardonnay berry collected 26 days after anthesis. Fluorescent cell walls are white and the non-fluorescent wall-enclosed spaces are black. Cell C_1 begins to close in slice (c) and disappears fully in slice (g). Cell C_2 begins to appear in slice (e). Only C_2 is visible in slices (g-i). Plasma membranes are visible within some cells indicating possible plasmolysis due to the fixation process.

Correcting the Confocal Z-Series for Signal Attenuation and Axial Distortion

Analysis of the z-series indicated the need to correct for signal attenuation. The number of black pixels per optical slice increased linearly with depth ($R^2 = 0.839$). This would cause an increase in the wall-enclosed area of 20% at 150 µm depth. A 20% increase in unit area would have led to to a 30% increase in unit volume and represented a serious potential for overestimating individual cell size. To minimise this error, attenuation of the fluorescent signal was corrected by sequentially increasing the intensity threshold. The corrected data displayed no fluorescence attenuation with depth, as indicated by regression analysis ($R^2 = 0.000$).

To check the extent of axial distortion within the confocal z-series, due to RI mismatch, the diameters of fluorescent microspheres were measured. The mean x/z ratio was 1.0445 (SD = 0.0205, n = 10), suggesting an axial compression of 4.45%. A multiplication factor of 1.0445 was applied to the z-series, changing the z-step from a nominal 1.0 µm to 1.0445 µm. As a consequence, the maximum image depth was expanded to 156.7 µm.

Comparison of Cell Wall Thickness (TEM vs CLSM)

The mean thickness of parenchyma cell walls obtained using transmission electron microscopy (TEM) was 97 nm (SD = 25.2 nm, n = 15). The mean cell wall thickness estimated from a stratified random sample within the confocal series was 940 nm (SD = 170 nm, n = 29). This discrepancy (843 nm) caused by excessive fluorescent emission within single confocal slices could have resulted in an underestimation of cell volume by as much as 15%. To approximate actual wall thickness the cell wall signal was eroded by one pixel (752 nm) to 188 nm. Further erosion was not possible.

Reconstructed Three-Dimensional (3D) Models of Cells and Cell Walls

Two-dimensional binary overlays of cell walls and wall-enclosed spaces from single optical slices were integrated to form 3D images. The 3D reconstructions of (a) cell walls and (b) 29 individual cells are shown in Figure 3. The size range for individual cells extended more than 14-fold, from 28 400 μm^3 to 411 000 μm^3 (mean = 143 000 μm^3, SD = 115 000 μm^3, n = 29). The population dynamics of the cells were represented graphically by plotting cell volume in ascending order (Figure 4). Groupings of cells around specific size classes were evident. Six distinct plateaux suggest the maximum size for a cell in that particular size class - 45 000 μm^3,

90 000 μm^3, 151 000 μm^3, 224 000 μm^3, 343 000 μm^3, and 411 000 μm^3. Note the decreasing interval between successive pairs of size class maxima. Cell shape was irregular and the planes of contact between cells were rarely flat or simple. Variability in cell shape was indicated by the range in surface area to volume ratios, from 0.080 to 0.198 μm^{-1}. Structural details greater than 1.5 µm were apparent at the internal surface of the cell wall. The regular, large undulations were artefacts, typical of integrated serial sections. The interconnected patterns of protuberances and invaginations appeared to be associated with the structure and position of internal cellular membranes. The more irregular, solitary protrusions may indicate the presence of primary pit fields.

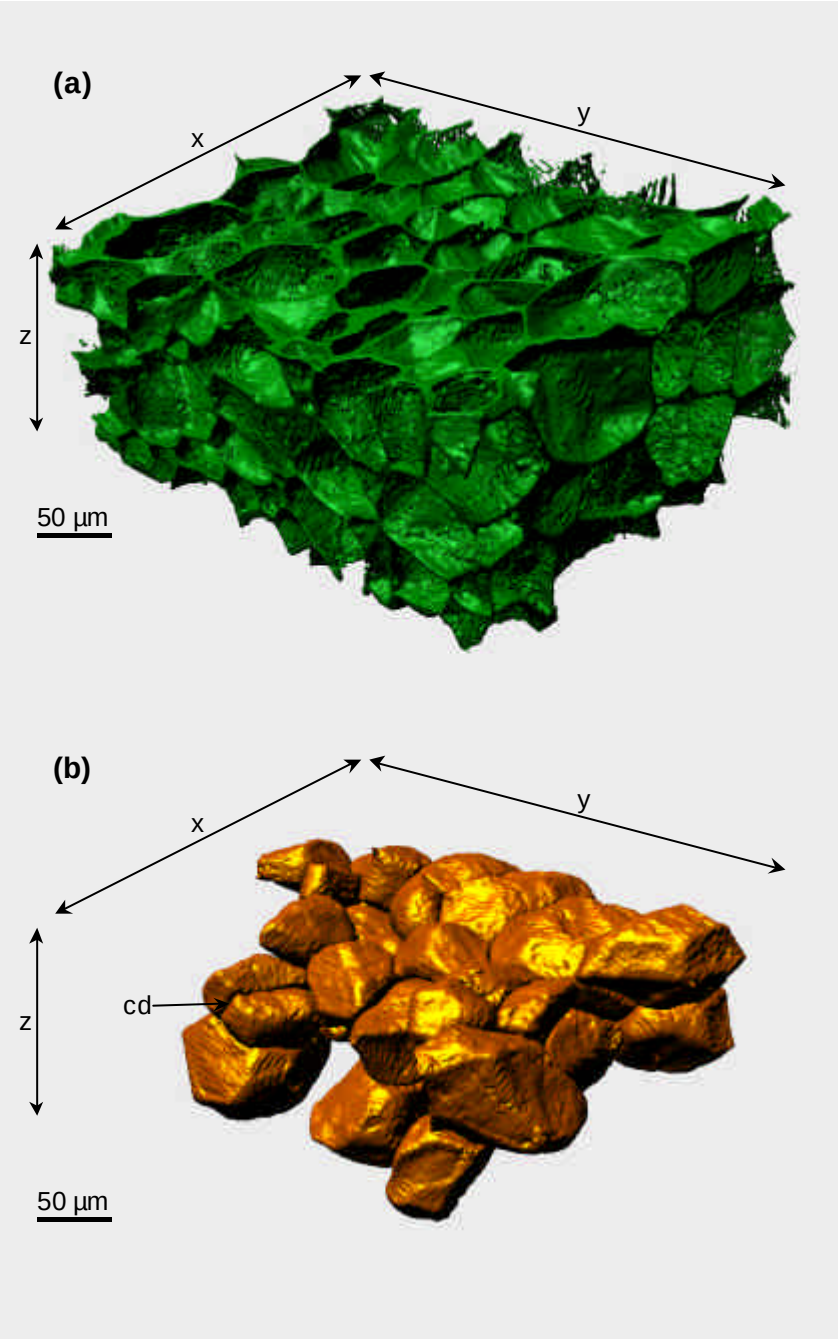


Figure 3. Parenchyma cell reconstructions. Digital 3D reconstruction of (a) cell walls prior to eroding and (b) 29 individual cells indicate the variety of shapes and sizes found among parenchyma cells in the inner mesocarp tissue of a Chardonnay berry harvested 26 days after flowering. Only entire cells are included, partial cells are excluded. A recent cell division is indicated at "cd".

Figure 4. Parenchyma cell volumes. Cell volumes of all 29 reconstructed parenchyma cells in Figure 3 from the inner mesocarp tissue of a Chardonnay berry harvested 26 days after flowering, grouped in ascending order. The curve suggests 6 distinct plateaux around particular size classes.

DISCUSSION

Techniques Used

Judicious, minimal cutting of the organ enabled the berry to maintain the integrity of its tissues, thus reducing the likelihood of cell distortion. This aspect of the project enabled individual cells to be viewed *in situ.*

The working distance of the objective lens (170 µm) proved to be the main limiting factor to the depth of tissue penetration in this experimental system. Although optical penetration was consistently high throughout the entire tissue, a high numerical aperture lens (NA = 1.4) was required to resolve cell walls running horizontal to the optical plane. This trade-off between working distance and numerical aperture in optical systems is unavoidable (Pawley, 1995). Larger volumes of tissue can be studied by aligning and combining adjacent z-series (Oldmixon and Carlsson, 1993): this increases the x and y dimensions of the scanned region, but z remains unchanged.

The use of fluorescent microspheres to derive a single empirical correction factor for axial distortion obviated the need for complex theoretical estimates involving geometric ray tracing models which often yield conflicting results (Visser and Oud, 1994; White *et al.*, 1996). This correction was only an approximation to what is theoretically a nonmonotonic function (Török *et al.*, 1997).

Cell wall thickness in confocal slices was greater than the estimates obtained using TEM. Confocal slices were deliberately over-saturated to ensure that all cell walls were visualised to a thickness of at least one pixel (0.752 µm). Attenuation of the fluorescent signal with depth caused cell walls to appear discontinuous on unsaturated slices. This was especially problematic for horizontal cell walls that emitted less fluorescence than their vertical counterparts. To avoid an under-estimation in the calculation of cell volume, each optical slice was corrected using a rank 3x3 filter which eroded the over-saturated cell walls by one pixel, thereby approaching the estimate of thickness obtained using TEM.

The 3D reconstruction software, ImageVolumes, was chosen on the grounds of the algorithm used, Marching Cubes, and its ability to visualise and measure structures imaged by CLSM. The merits of available 3D packages and algorithms are discussed in White (1995).

Shapes and Sizes of Parenchyma Cells

Contemporary 3D reconstruction techniques in plant biology are infrequent (Knoblauch and van Bel, 1998; Travis *et al.*, 1997; White *et al.*, 1996) although many of the stereological principles were established by botanists earlier this century. The group of 29 cells visualised here, or each cell individually, can be viewed on screen from all angles. Measurements can be made of volume, surface area, surface morphology, and the number of surface planes.

The final resolution of the reconstructed images is a function of the optical, digital and rendering resolution of the imaging system. Optical resolution is determined by the excitation wavelength (λ = 488 nm) and the numerical aperture (NA = 1.4) of the lens. It varies in the x-y (0.174 µm) and z (~ 0.5µm) planes. Digital resolution is prescribed by the CCD in combination with lens magnification (0.376 µm / pixel) and post-collection modifications to the data (0.752 µm / pixel after combining z-series). Rendering resolution in the x-y plane is twice the unit pixel size (1.504 µm), but rendering resolution in z-axis is the distance between the optical slices (1.0445 µm). Each voxel therefore represents 2.36 μm^3. This number represents

the precision of *in situ* volume measurements for individual, whole parenchyma cells within a block of grape berry mesocarp tissue.

The mean size found for grape mesocarp cells at this stage of development compares favourably with published sources (Considine and Knox, 1981; Coombe, 1976; Harris *et al.*, 1968) but the range and variability have not previously been described. The indication of a succession of size classes deserves further study. Such classes might represent developmental cohorts of cells, where the smaller cells have arisen as mitotic divisions of the larger cells. The decreasing interval between successive cohorts suggest asynchronous divisions of different sized cells.

A study of the shape of individual cells could be developed from these results. Cell shape in space-filling tissues is described by the planes of contact (facets) with neighbouring cells. In homogeneous, space-filling tissues, the mean number of facets per cell is said to approach 14. This is true of some plant cells, soap bubbles and compressed metal grains (Williams, 1968). The orthic tetrakaidecahedron, a geometrically perfect 14-sided polyhedron with 8 hexagonal and 6 quadrilateral faces, was proposed as the archetypal shape for parenchyma cells (Kelvin, 1887; Korn, 1974; Korn and Spalding, 1973; Matzke, 1948; Thompson, 1942), but this form is rarely achieved in nature due to the occurrence of varying cell sizes within a developing tissue (Matzke and Duffy, 1956). Where both small and large cells are present in the same tissue, it is obligatory for the larger cells to have more facets than the smaller cells. The relevance of mean number of facets per cell as a quantitative descriptor of cell size is questionable, given that cell contacts are not always flat, planar surfaces. It is less precise than the absolute measurements of cell volume, surface area and shape obtained in the present study.

The technique described in this paper for measuring and visualising plant parenchyma cells in 3D using whole mounts of cleared, stained tissue in conjunction with CLSM and digital 3D reconstruction is applicable to a wide range of morphometric analyses in plant cell biology. It could be a valuable complement to molecular genetics for elucidating factors critical to the development of plant form and function.

EXPERIMENTAL PROCEDURES

Tissue Preparation

Grape berries were sampled from *Vitis vinifera* L. cv. Chardonnay vines, 26 days after anthesis had commenced. The tissue of interest in this study was the parenchymatous inner mesocarp of the grape berry consisting of about 10 layers of large, highly vacuolated cells. Berries were fixed in FPA_{50} and stored in 70% ethanol. Individual berries were bisected longitudinally using a razor blade fragment. The half-berries were used in two ways: first, for testing of stains using thin, embedded sections; secondly, for confocal microscopy without further cutting.

Berry halves were dehydrated through an alcohol series, infiltrated with GMA, embedded in GMA in gelatin capsules and oven-cured according to Feder and O'Brien (1968). Sections of 2 µm thickness were checked for autofluorescence and treated with one of the following stains: acridine orange, aniline blue, aniline blue fluorochrome, Calcofluor White M2R, Congo red, coriphosphine O, euchrysine 2GNX, Evans blue, FITC, magdala red, periodic acid-Schiff's, Ponceau S, pontamine sky blue, resorcin blue, safranin O, trypan blue. Stained sections were visualised under a fluorescence microscope.

Clearing of half-berries was explored after it was found that untreated tissue was too opaque to allow sufficient penetration of laser light. Mounting the tissue in a medium of higher RI increases optical penetration. The RI of parenchyma cells approximates that of water [RI ~ 1.33] (O'Brien and McCully, 1981). Several highly refractive immersion media were tested in this study: glycerol [RI ~ 1.47], xylene [RI ~ 1.50], methyl benzoate [RI ~ 1.52], and methyl salicylate [RI ~ 1.54]. More destructive clearing techniques were also tested: mounting the tissue directly in 80% lactic acid at 50-60°C (Simpson, 1929) and the use of specialised mixtures (Herr, 1971; 1982). Methyl salicylate was selected.

The following protocol was adopted: berry halves were dehydrated under vacuum through an ethanol series, cleared in methyl salicylate, stained with 0.5% safranin O in methyl salicylate and mounted, cut face down, on a glass coverslip in a well constructed of a ring of silicone rubber filled with methyl salicylate (Figure 1). The further work consisted of examination of the visualised tissue zone, illustrated in Figure 1.

Confocal Laser Scanning Microscopy (CLSM)

Confocal images of the cell walls were collected using a BioRad MRC-1000 uv confocal system attached to a Nikon Diaphot-300 inverted microscope. The objective lens was a Nikon 60x oil immersion plan apochromat with a numerical aperture of 1.4 and a working distance of 170 µm. A krypton/argon laser was used to excite the specimen at 488/10 nm and emission was collected at 522/35 nm with the confocal aperture closed down to 1.5 mm. A sequence of 151 x-y optical slices was collected, each with a 1.0 µm separation on the z-axis. Images from a 289 x 193 µm field-of-view (768 x 512 pixels) were captured as computer files. Fluorescent intensity was digitally coded using 256 levels of grey, with 0 representing the lowest intensity (black) and 255 the highest (white). The cell wall intensity was deliberately oversaturated to compensate for reduced fluorescence in deeper parts of the tissue. Two neighbouring z-series were combined post-collection thus doubling the volume of tissue examined and increasing the number of cells included in the analysis. The combined field-of-view was 289 x 385 µm (384 x 512 pixels).

Calibration of Intensity Attenuation with Depth

Signal attenuation is a function of absorption and scattering of both excitation and emission light (Guilak, 1994; Rigaut and Vassy, 1991). In the present study, the collected fluorescent signal represented cell walls, whereas the unstained cell interior appeared black. Lessening of the fluorescent signal deriving from the cell walls could result in an overestimation of the true size of the cell.

A binary threshold that qualitatively separated cell walls (white pixels) from cells (black pixels) was used to assess signal attenuation. The number of black pixels in each optical slice of the combined image stack was plotted against slice depth using NIH Image analysis software (Version 1.61 U.S. National Institute of Health, 1996). Attenuation increased linearly with depth so an intensity threshold correction factor was sought to minimise its impact on cell size calculations. An incremental threshold adjustment which yielded a regression line of zero slope was used to recalculate intensity thresholds for each optical slice.

Calibration of Axial Distortion

Some degree of axial distortion in the z-axis was anticipated on the basis of the RI mismatch between the lens immersion medium (oil RI = 1.5124 @ 22.5°C) and the specimen mounting medium (methyl salicylate RI = 1.5358 @ 22.5°C) (Carlsson, 1991; Hell *et al.*, 1993). This was calibrated with nominal 10 µm yellow-green fluorescent microspheres composed of a polystyrene envelope containing a fluorescent dye. Confocal, non-saturated, vertical sections of 10 microspheres mounted in methyl salicylate were collected using the same filter set as the berry images. The x and z diameters of the spheres were determined as the distance between the edges of the spheres located at 50% of the greyscale intensity threshold between the centre of the microsphere and the adjacent background. A correction factor of 4.5% was calculated using the ratio of x to z diameter of microspheres.

Transmission Electron Microscopy (TEM) of Cell Walls

Cell wall thickness was verified using TEM. Berry tissue was post-fixed in 2% osmium tetroxide, dehydrated through an acetone series, infiltrated with an araldite embedding resin, embedded in fresh resin and polymerised under vacuum at 70°C (Mollenhauer, 1964). Sections of 70 nm thickness were cut on an ultramicrotome, stained with 5% uranyl acetate in 70% ethanol and Reynolds' lead citrate, and mounted on an aluminium grid. The sections were visualised under TEM and cell wall thickness was estimated from a stratified random sample. Differences in cell wall thickness between TEM and CLSM were corrected by applying a rank 3x3 filter to erode cell walls by one pixel in each optical slice.

Three-Dimensional (3D) Reconstruction

To visualise the confocal data, ImageVolumes (Version 3.0 Minnesota Datametrics Corporation, 1994) software run on a Silicon Graphics Indigo 2 computer under the Irix 5.3 operating system was used. Cell walls and cells were reconstructed from the z-series using two-dimensional binary overlays of the cell walls and wall-enclosed spaces. These overlays were integrated in the axial dimension by the Marching Cubes algorithm (Lorensen and Cline, 1987), a surface-based technique used to render 3D images from voxel data by forming isointensity contours of the object surface. Image rendering, smoothing and lighting techniques

allowed individual cells to be viewed as geometric solids. Cells were reconstructed only if they were fully enclosed within a continuous cell wall (i.e. only entire cells were considered, partial cells were ignored).

Cell surface area and volume were measured with a distance field analysis software package (Dfield Version 2.0 Minnesota Datametrics Corporation, 1994) which calculated 3D scalar quantities whose values described the Euclidean distance from any given point in space at Cartesian coordinates (x,y,z) to the closest surface of the 3D model.

ACKNOWLEDGEMENTS

The Australian Research Council, the Grape and Wine Research and Development Corporation and Southcorp Wines Pty Ltd are gratefully acknowledged for their financial support. We thank the following: Ian Gibbins and Grant Hennig from the Department of Anatomy and Histology, the Flinders University of South Australia, for access to the SGI Indigo 2 computer and 3D software; Marilyn Henderson from the Centre for Electron Microscopy and Microstructural Analysis, the University of Adelaide, for assistance with the TEM analysis; Prue Henschke from C.A. Henschke and Co., for providing the grape material; and Nick S. White from the Department of Plant Sciences, the University of Oxford, for commenting on a draft of the manuscript.

REFERENCES

Bron, Cph., Gremillet, Ph., Launay, D., Jourlin, M., Gautschi, H.P., Bächi, Th. and Schüpbach, J. (1990) Three-dimensional electron microscopy of entire cells. *J. Microsc.* **157,** 115-126.

Carlsson, K., Danielsson, P.E., Lenz, R., Liljeborg, A., Majlöf, L. and Åslund, N. (1985) Three-dimensional microscopy using a confocal laser scanning microscope. *Opt. Lett.* **10,** 53-55.

Carlsson, K. (1991) The influence of specimen refractive index, detector signal integration, and non-uniform scan speed on the imaging properties in confocal microscopy. *J. Microsc.* **163,** 167-178.

Considine, J.A. (1978) Stereology of the dermal system of fruit. *J. Microsc.* **113,** 61-68.

Considine, J.A. (1981) Stereological analysis of the dermal system of the fruit of the grape *Vitis vinifera* L. *Aust. J. Bot.* **29,** 463-474.

Considine, J.A. and Knox, R.B. (1981) Tissue origins, cell lineages and patterns of cell division in the developing dermal system of the fruit of *Vitis vinifera*. L. *Planta,* **151,** 403-412.

Coombe, B.G. (1976) The development of fleshy fruits. *Ann. Rev. Plant Physiol.* **27,** 207-228.

Cruz-Orive, L.M. (1997) Stereology of single objects. *J. Microsc.* **186,** 93-107.

Feder, N. and O'Brien, T.P. (1968) Plant microtechnique: some principles and new methods. *Am. J. Bot.* **55,** 123-142.

Guilak, F. (1994) Volume and surface area measurement of viable chondrocytes *in situ* using geometric modelling of serial confocal sections. *J. Microsc.* **173,** 245-256.

Harris, J.M., Kriedemann, P.E. and Possingham, J.V. (1968) Anatomical aspects of grape berry development. *Vitis,* **7,** 106-119.

Hell, S., Reiner, G., Cremer, C. and Stelzer, E.H.K. (1993) Aberrations in confocal fluorescence microscopy induced by mismatches in refractive index. *J. Microsc.* **169,** 391-405.

Herr, J.M., Jr. (1971) A new clearing-squash technique for the study of ovule development in angiosperms. *Am. J. Bot.* **58,** 785-790.

Herr, J.M., Jr. (1982) An analysis of methods for permanently mounting ovules cleared in four-and-a-half type clearing fluids. *Stain Tech.* **57,** 161-169.

Kelvin, Lord. (1887) On the division of space with minimum partitional area. *Phil. Mag.* **24,** 503-514.

Knoblauch, M. and van Bel, A.J.E. (1998) Sieve tubes in action. *Plant Cell,* **10,** 35-50.

Korn, R.W. (1974) The three-dimensional shape of plant cells and its relationship to pattern of tissue growth. *New Phytol.* **73,** 927-935.

Korn, R.W. and Spalding, R.M. (1973) The geometry of plant epidermal cells. *New Phytol.* **72,** 1357-1365.

Lewis, F.T. (1926) The effect of cell division on the shape and size of hexagonal cells. *Anat. Rec.* **33,** 331-355.

Lorensen, W.E. and Cline, H.E. (1987) Marching cubes: a high resolution 3D surface construction algorithm. *Comp. Graphics,* **21,** 163-169.

Matzke, E.B. (1948) The three-dimensional shape of epidermal cells of the apical meristem of *Anacharis densa* (Elodea). *Am. J. Bot.* **35,** 323-332.

Matzke, E.B. and Duffy, R.M. (1956) Progressive three-dimensional shape changes of dividing cells within the apical meristem of *Anacharis densa*. *Am. J. Bot.* **43,** 205-225.

Mollenhauer, H.H. (1964) Plastic embedding mixtures for use in electron microscopy. *Stain Tech.* **39,** 111-114.

Møller, A., Strange, P. and Gundersen, J.G. (1990) Efficient estimation of cell volume using the nucleator and the disector. *J. Microsc.* **159,** 61-71.

O'Brien, T.P. and McCully, M.E. (1981) *The Study of Plant Structure: Principles and Selected Methods.* Melbourne: Termarcarphi.

Oldmixon, E.H. and Carlsson, K. (1993) Methods for large data volumes from confocal scanning laser microscopy of lung. *J. Microsc.* **170,** 221-228.

Parsons, D.F., Cole, R.W. and Kimelberg, H.K. (1989) Shape, size, and distribution of cell structures by 3D graphics reconstruction and stereology. *Cell Biophys.* **14,** 27-42.

Pawley, J.B. (ed.) (1995) *Handbook of Biological Confocal Microscopy* 2nd Edn. New York: Plenum Press.

Rigaut, J.P. and Vassy, J. (1991) High resolution three-dimensional images from confocal scanning laser microscopy. Quantitative study and mathematical correction of the effects due to bleaching and fluorescence attenuation in depth. *Anal. Quant. Cytol. Histol.* **13,** 223-232.

Simpson, J.L.S. (1929) A short method of clearing plant tissues for anatomical studies. *Stain Tech.* **4,** 131-132.

Thompson, D'Arcy W. (1942) *On Growth and Form* 2nd Edn. Cambridge: Cambridge University Press.

Török, P., Hewlett, S.J. and Varga, P. (1997) The role of specimen-induced spherical aberration in confocal microscopy. *J. Microsc.* **188,** 158-172.

Travis, A.J., Murison, S.D., Perry, P. and Chesson, A. (1997) Measurement of cell wall volume using confocal microscopy and its application to studies of forage degradation. *Ann. Bot.* **80,** 1-11.

Underwood, E.E. (1970) *Quantitative Stereology*. Massachusetts: Addison-Wesley Publishing Co..

Visser, T.D. and Oud, J.L. (1994) Volume measurements in three-dimensional microscopy. *Scanning,* **16,** 198-200.

Weibel, E.R. (1979) *Stereological Methods* Volume 1. *Practical Methods for Biological Morphometry*. London: Academic Press.

Weibel, E.R. (1980) *Stereological Methods* Volume 2. *Theoretical Foundations*. London: Academic Press.

White, N.S., Errington, R.J., Fricker, M.D. and Wood, J.L. (1996) Aberration control in quantitative imaging of botanical specimens by multidimensional fluorescence microscopy. *J. Microsc.* **181,** 99-116.

White, N.S. (1995) Visualisation systems for multidimensional CLSM images. In *Handbook of Biological Confocal Microscopy* 2nd Edn. (Pawley, J.B. ed.). New York: Plenum Press, pp. 211-254.

Williams, R.E. (1968) Space-filling polyhedron: its relation to aggregates of soap bubbles, plant cells, and metal crystallites. *Science,* **161,** 276-277.

Williams, R.F. (1970) The genesis of form in flax and lupin as shown by scale drawings of the shoot apex. *Aust. J. Bot.* **18,** 167-173.

Yu, R.C., Abrams, D.C., Alaibac, M. and Chu, A.C. (1994) Morphological and quantitative analyses of normal epidermal Langerhans cells using confocal scanning laser microscopy. *Brit. J. Dermat.* **131,** 843-848.